#1131 IGARSS 2014

Characterization of oceanic mesoscale and sub-mesoscale energy spectra and fluxes

Sung Yong Kim†

Division of Ocean Systems Engineering, School of Mechanical, Aerospace & Systems Engineering, Korea Advanced Institute of Science and Technology
syongkim@kaist.ac.kr†

Abstract

Oceanic submesoscale processes are crucial for yielding the vertical transport of tracers, mass, and buoyancy and for rectifying the mixed layer structure and upper ocean stratification. However, their observational studies have been rarely substantiated because they require high-resolution in-situ measurements in time and space. Here we examine the oceanic energy spectra and their fluxes at submesoscale with oceanic currents, observed from multiple platforms of satellite altimeters, shore-based high-frequency radars, shipboard acoustic doppler current profilers, in order to characterize submesoscale processes. Our results confirm that oceanic energy spectra decay with a slope of -2 at the scale of $O(1)$ km in the one-dimensional wavenumber domain, and their inverse cascade appears at the length scale of $O(1)$ km. We conclude that oceanic energy at submesoscale is clearly determined at the scales below the observational limit of present-day satellite altimeters.

Data Analysis

The HFR-derived hourly surface currents with 1, 6, and 20 km spatial resolutions off the U.S. West Coast (USWC) over two years (2008 to 2009) are analyzed [e.g., [1]]. The HFR surface currents contain various aspects of coastal surface circulation averaged over upper one meter depth including poleward- or equatorward-propagating signals near the coast, near-inertial oscillations, surface tide-coherent currents, local and remote wind-forced circulation, intermittent and persistent submesoscale and mesoscale eddies, and surface modulations due to internal waves and tides.

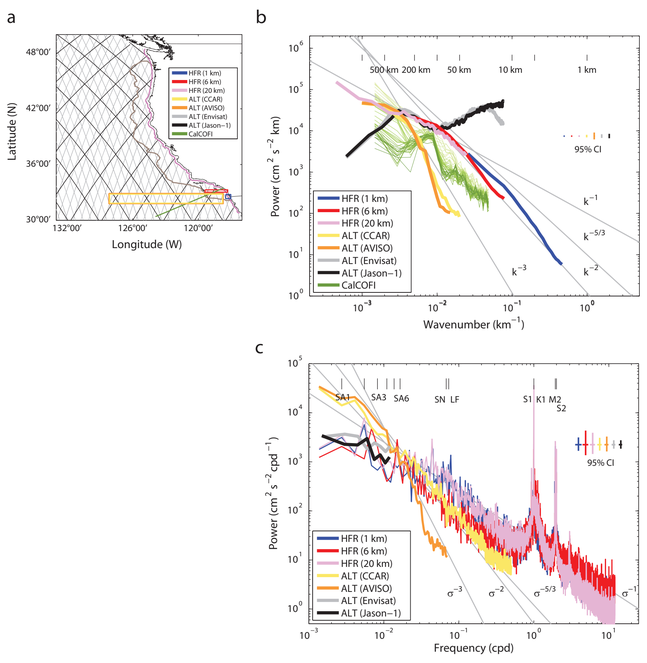

Figure 1: A study domain for continuity of ocean surface scales off the USWC. Sampling locations of HFR surface currents with three spatial resolutions (1, 6, and 20 km), ALT gridded geostrophic currents (CCAR and AVISO), ALT along-track SSHAs (Envisat and Jason-1), and a CalCOFI cruise track (Line 90) are indicated. The effective coverage of HFR surface currents is denoted by a dark gray curve. (b) and (c): Power spectra of high-frequency radar-derived (HFR; 1, 6, and 20 km resolutions) surface currents and altimeter-derived geostrophic currents [ALT; optimally interpolated current products of CCAR (∼25 km resolution) and AVISO (∼33 km resolution) and along-track Envisat and Jason-1] for two years (2007 and 2008) in the (b) wave-number domain [Length scales (L) of 1, 5, 10, 50, 100, 200, 500, and 1000 km are marked] and (c) frequency domains [Six seasonal harmonics (SA_1 to SA_6), spring-neap (SN, 14.765-day), lunar fortnightly (LF, 13.661-day), S_1, K_1, M_2, and S_2 tidal frequencies are marked]. The wave-number spectra of shipboard ADCP currents in quarterly CalCOFI cruises (1993 to 2004) in vertical are shown as light green (shallow; at 16 m depth) to dark green (deep, 408 m depth) curves.

Four kinds of products of ALT-derived geostrophic currents in the northeastern Pacific (30°N to 50°N, 114°W to 133°W) are examined (Figure 1a). Two sets of 7-daily along-track sea surface height anomalies (SSHAs) with respect to the seven-year mean dynamic topography from Envisat and Jason-1 are analyzed. Two gridded products of the Colorado Center for Astrodynamics Research (CCAR) daily geostrophic currents with a quarter degree resolution and the AVISO 7-daily geostrophic currents with approximately one-third degree resolution are considered.

Subsurface currents observed from the shipboard ADCP in quarterly California Cooperative Fisheries Investigation (CalCOFI) cruises for 12 years (1993 to 2004) are analyzed. Although this data set is not overlapped with HFR and ALT data, it will provide typical energy spectra of subsurface currents.

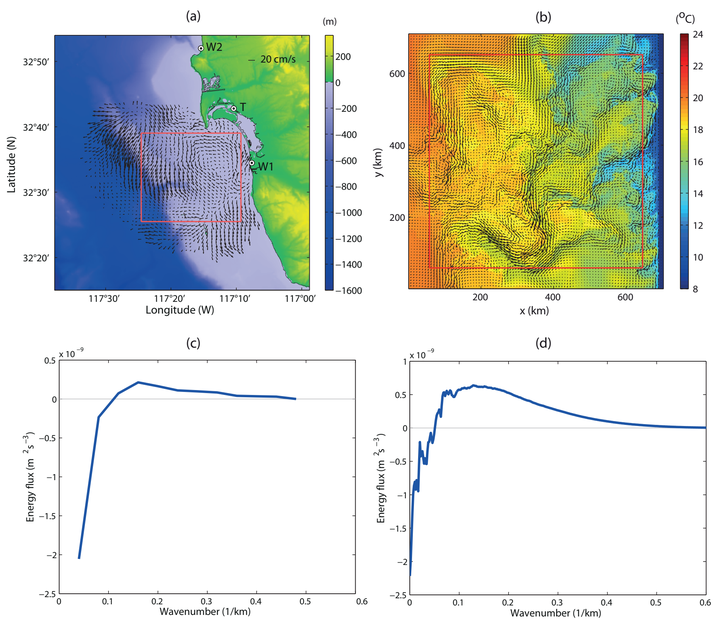

Figure 2: (a) A single map of observed surface currents with a 1 km spatial resolution (San Diego). (b) A single map of the surface currents and surface temperature obtained from a numerical model with a 0.75 km spatial resolution [2]. (c) and (d): Advective energy fluxes computed from the observation and model (Courtesy of X. Capet; [2]).

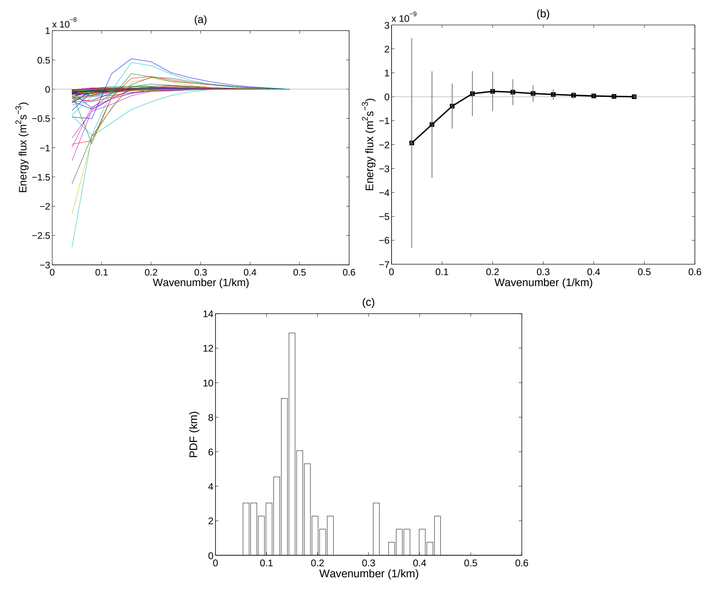

Figure 3: Energy fluxes are estimated from daily averaged surface current fields over two years (2003 to 2005). We consider only cases to satisfy both conditions: 1) the KE flux at the lowest wavenumber is negative and 2) there is only a single cross-crossing. (a) Whole plots of the chosen 88 cases out of 731. (b) Averaged KE flux. (c) PDF of the zero-crossing wavenumber.

The one-dimensional wavenumber spectra of HFR surface currents at three spatial resolutions (1, 6, and 20 km) show consistent and continuous energy distribution ranging from $O(1000)$ km to $O(1)$ km. Most of them decay with k^{-2} at high wavenumber in agreement with typical submesoscale energy spectra (Figure 1b). While driving forces of circulation and partitioning of both geostrophic and ageostrophic components may vary regionally and appear in energy spectra, the estimated energy spectra have a robust k^{-2} behavior. The energy spectra of ALT cross-track currents at scales larger than 100 km ($L > 100$ km) agree with those of HFR surface currents and show observational limits of present-day satellite ALT at scales below 100 km scale. As the HFR surface currents off southern California contain a minimum ageostrophic currents (e.g., wind-driven components), their power spectra are comparable to the spectra of ALT cross-track geostrophic currents (Envisat and Jason-1) (Figure 1b). The variance difference at low wavenumber ($L > 500$ km) in the HFR and along-track ALT observations results from existence of alongshore signals with large wavelength near the coast (e.g., coastally trapped waves). As HFR surface currents were sampled in the cross-shore (1 and 6 km resolutions) and along-shore directions (20 km resolution), the energy spectra may contain coastal boundary effects due to bathymetry and shoreline. The one-dimensional wavenumber spectrum with a slope of k^{-2} (or two-dimensional wavenumber spectrum with a slope of k^{-3}) is related to the exponential covariance function in the physical space.

Since HFR-derived surface currents contain responses to primary geophysical forces such as tides, winds and their interactions, the KE fluxes of surface currents can be interpreted in terms of those driving forces. Furthermore, considering the Nyquist wavenumber and availability of concurrent in-situ observations (e.g., tides and winds), we decide to examine the hourly surface current maps with 1 km resolution off southern San Diego, which have been carefully addressed in terms of decomposing analysis of surface currents and their spatial structures.

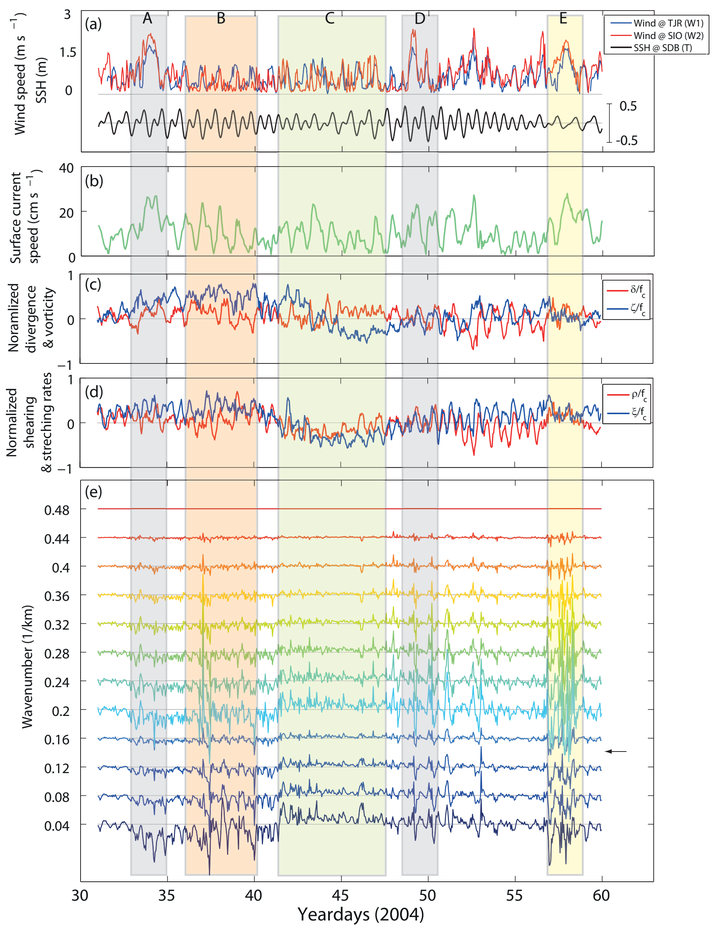

Figure 4: (a) Time series of local winds at Tijuana River Valley (TJR; W1) and Scripps Pier (SIO; W2) and sea surface elevation at San Diego Bay (SDB; T) (Figure 2a). (b) to (d): Time series of the spatially averaged kinematic and dynamic quantities estimated from HFR-derived surface currents within a red box in Figure 2a. (b) Magnitudes of surface currents. (c) Divergence (δ/f_c) and vorticity (ζ/f_c) normalized by the local Coriolis frequency. (d) Shearing deformation rate (ρ/f_c) and stretching deformation rates (ξ/f_c) normalized by the local Coriolis frequency. (e) Time series of advective energy fluxes [$\Pi^*(k^*, t)$] at each wavenumber estimated from HFR-derived surface currents within a red box (Figure 2a). Both strong winds and spring tide (A and D), spring tide only (B), positive advective KE fluxes at low wavenumber (C), and enhanced fluctuations of KE fluxes with local wind dominance (E) are taken into account.

Examples of advective KE fluxes [$\Pi^*(k^*, t)$] are presented in a systematic way. First, as a feasibility check, we compare the KE fluxes estimated from the daily averaged surface current map during a wind-dominant period and the surface current map obtained from wind stress-forced numerical simulations (Figure 2). Secondly, in order to examine the influence of regional driving forces on the advective KE fluxes, the time series of KE fluxes at each wavenumber estimated from hourly HFR-derived surface current maps are investigated (Figures 3 and 4).

Figures 2a and 2b present examples of surface currents observed from HFRs off southern San Diego (1 km resolution) and obtained from submesoscale numerical simulations, forced by wind stress (0.75 km resolution) [e.g., [2]], respectively. The range (e.g., maximum and minimum) of the KE fluxes estimated from two data sets is different, however, the length scales to divide forward cascade (positive KE) and backward cascade (negative KE) are comparable, appearing between 8 and 15 km (Figures 2c and 2d).

Acknowledgement

Sung Yong Kim is supported by the Human Resources Development of the Korea Institute of Energy Technology Evaluation and Planning (KETEP), Ministry of Trade, Industry and Energy (No. 20114030200040).

References

[1] S. Y. Kim, E. J. Terrill, B. D. Cornuelle, B. Jones, L. Washburn, M. A. Moline, J. D. Paduan, N. Garfield, J. L. Largier, G. Crawford, and P. M. Kosro. Mapping the U.S. West Coast surface circulation: A multiyear analysis of high-frequency radar observations. *J. Geophys. Res.*, 116, 2011.

[2] X. Capet, J. C. McWilliams, M. J. Molemaker, and A. F. Shchepetkin. Mesoscale to submesoscale transition in the California Current System. Part I: Flow structure, eddy flux, and observational tests. *J. Phys. Oceanogr.*, 38(1):29–43, 2008.